Critical role of glioma-associated oncogene homolog 1 in maintaining invasive and mesenchymal-like properties of melanoma cells

	Gunarta I Ketut, Li Rong, Nakazato Ryota, Suzuki Ryusuke, Boldbaatar Jambaldorj, Suzuki Takeshi, Yoshioka Katsuji
journal or publication title	Cancer Science
volume	108
number	8
page range	1602-1611
year	2017-08-01
URL	http://hdl.handle.net/2297/48456

Critical role of glioma-associated oncogene homolog 1 in maintaining invasive and mesenchymal-like properties of melanoma cells

I Ketut Gunarta,[1] Rong Li,[1] Ryota Nakazato,[1] Ryusuke Suzuki,[1] Jambaldorj Boldbaatar,[1] Takeshi Suzuki[2] and Katsuji Yoshioka[1] (ID)

Divisions of [1]Molecular Cell Signaling; [2]Functional Genomic, Cancer Research Institute, Kanazawa University, Kanazawa, Japan

Cutaneous melanoma is the most aggressive form of skin cancer. This aggressiveness appears to be due to the cancer cells' ability to reversibly switch between phenotypes with non-invasive and invasive potential, and microphthalmia-associated transcription factor (MITF) is known to play a central role in this process. The transcription factor glioma-associated oncogene homolog 1 (GLI1) is a component of the canonical and noncanonical sonic hedgehog pathways. Although GLI1 has been suggested to be involved in melanoma progression, its precise role and the mechanism underlying invasion remain unclear. Here we investigated whether and how GLI1 is involved in the invasive ability of melanoma cells. *Gli1* knockdown (KD) melanoma cell lines, established by using *Gli1*-targeting lentiviral short hairpin RNA, exhibited a markedly reduced invasion ability, but their MITF expression and activity were the same as controls. *Gli1* KD melanoma cells also led to less lung metastasis in mice compared with control melanoma cells. Furthermore, the *Gli1* KD melanoma cells underwent a mesenchymal-to-epithelial-like transition, accompanied by downregulation of the epithelial-to-mesenchymal transition (EMT)-inducing transcription factors (EMT-TF) *Snail1*, *Zeb1* and *Twist1*, but not *Snail2* or *Zeb2*. Collectively, these results indicate that GLI1 is important for maintaining the invasive and mesenchymal-like properties of melanoma cells independent of MITF, most likely by modulating a subset of EMT-TF. Our findings provide new insight into how heterogeneity and plasticity are achieved and regulated in melanoma.

Malignant melanoma represents a small percentage of skin cancers, but is the major cause of death from these cancers.[1,2] Melanoma arises from melanocytes (pigment cells), and approximately 50% of melanomas harbor the activating BRAF[V600E] mutation.[3] Although small molecule inhibitors targeting BRAF and MEK, a downstream effector of BRAF, are effective in BRAF-mutated melanoma, virtually all of the tumors develop resistance to the drugs, usually within a few months.[4–10] Immune checkpoint inhibitors, such as an anti-programmed death 1 (PD-1) antibody, provide durable responses in patients with metastatic melanoma independent of the BRAF mutational status; however, a significant proportion of patients either do not respond or develop resistance to the PD-1 immunotherapy.[11–15]

Tumor heterogeneity poses a major challenge for the effective treatment of cancer. Accumulating evidence indicates that the heterogeneity in melanoma can be driven through phenotypic plasticity.[16–18] That is, the aggressiveness of melanoma appears to be due to the cancer cells' ability to reversibly switch between different phenotypes with non-invasive and invasive potential. Microphthalmia-associated transcription factor (MITF) plays an essential role in determining the melanocyte lineage and has been proposed to act as a rheostat for the

cellular heterogeneity in melanoma.[17,19,20] In the rheostat model, low levels of MITF generate invasive, stem-like cells, whereas high MITF levels stimulate proliferation and inhibit invasion. Epithelial-to-mesenchymal transition (EMT) is a dynamic and reversible phenotypic switching process where polarized epithelial cells transition to motile mesenchymal cells; this process is essential for normal development and is widely thought to be a critical switch for tumor-cell invasiveness.[21–23] EMT is driven by an interconnected signaling network of EMT-inducing transcription factors (EMT-TF), including SNAIL, TWIST and ZEB. Recent studies have shown that some EMT-TF play important roles in malignant melanoma, but their regulation and function are different from those in epithelial cancers.[24,25] These studies also suggest that the EMT-TF SNAIL2 and ZEB2 act as tumor-suppressor proteins by activating an MTIF-dependent melanocyte differentiation program.

Sonic hedgehog (Shh) signaling has critical roles in embryonic patterning, and aberrant Shh-signaling activation is implicated in various cancer types, including skin cancer.[26–29] The Shh signal is transduced by a receptor complex composed of two proteins, Patched (PTCH) and Smoothened (SMO). The binding of Shh to PTCH relieves PTCH's repression of SMO.

The transcription factor glioma-associated oncogene homolog 1 (GLI1) acts as a terminal, positive effector of Shh signaling, and *Gli1* itself is a Shh-target gene. GLI1's expression and activity are also regulated through a non-canonical Shh pathway, such as those involving hypoxia or transforming growth factor (TGF)-β.[30–32] GLI1 has been suggested to be involved in melanoma progression, although its precise role and the mechanism underlying invasion remain unclear. In this study, we show that GLI1 has a role in maintaining the invasive and mesenchymal-like properties of melanoma cells.

Materials and Methods

Cell culture. B16F10 murine melanoma cells were obtained from Riken BioResource (Tokyo, Japan), and MeWo and G361 human melanoma cells from JCRB Cell Bank (Osaka, Japan). B16F10 cells were cultured in RPMI 1640 medium (Nissui Pharmaceutical, Tokyo, Japan) supplemented with 10% FBS, and MeWo and G361 cells in Eagle's Minimum Essential Medium (EMEM) with non-essential amino acids (Wako, Tokyo, Japan) and 10% FBS. To prepare conditioned medium, NIH3T3 cells, a kind gift from Dr Chiaki Takahashi (Kanazawa University, Kanazawa, Japan), were cultured in RPMI 1640 (Nissui Pharmaceutical) supplemented with 10% FBS. Mouse embryonic fibroblasts (MEF) and HEK293T cells were cultured as described previously.[33] In some experiments, cyclopamine (LKT Labs, St. Paul, MN, USA) and forskolin (Wako) were DMSO and added to the culture medium (see Figs 1 and S1).

Plasmids, viral vector preparation, and viral infection. The pLVTH lentivirus plasmid vectors for shRNA were constructed as previously described.[34] In pLVTH, enhanced green fluorescent protein (EGFP) is encoded as a marker. Previously reported target sequences, which are listed in Table S1, were used to express shRNA against mouse *Gli1*, human *Gli1* and firefly *Luciferase* (*Luc*). Lentiviral vectors were produced as previously described.[34] B16F10, MeWo and G361 cells were infected with the lentiviruses, and were analyzed at 7 days post-infection (dpi). The mammalian expression plasmid pCL20c-CMV-EGFP was described previously.[34] The coding regions of full-length mouse GLI1 with hemagglutinin (HA) tag sequences at the 5′ and 3′ ends were inserted into pCL20c-CMV[34] to generate pCL20c-CMV-HA-GLI1 and pCL20c-CMV-GLI1-HA, respectively. The potential promoter regions of *Snail1*, *Zeb1* and *Twist1* were obtained by PCR using B16F10 genomic DNA as templates. The PCR products were subcloned into a promoterless pGL3 vector (Promega, Madison, WI, USA). All PCR products were verified by sequencing.

Western blot analysis. Total cell lysates were prepared and analyzed by western blotting as previously described,[34] using rabbit anti-GLI1 H300 (sc-20687), rabbit anti-E-cadherin H108 (sc-7870; each diluted to 1:1000; Santa Cruz Biotechnology, Santa Cruz, CA, USA), rabbit anti-MITF N2C1 (1:1000; GTX113776; GeneTex, Irvine, CA, USA), and mouse anti-α-tubulin (1:3000; #T5168; Sigma-Aldrich, St. Louis, MO, USA) antibodies (Abs).

Quantitative reverse-transcription PCR. Total RNA was prepared and qRT-PCR was performed as previously described.[35] Primers used for qRT-PCR are listed in Table S2.

Phalloidin staining and immunocytochemistry. Phalloidin staining was carried out as described previously.[36] Immunocytochemistry was performed following standard protocols as

previously described,[34] using the rabbit anti-E-cadherin H108 (1:200; Santa Cruz Biotechnology) Ab. The secondary Ab was goat Alexa fluor 568-conjugated anti-rabbit IgG Ab (1:1000; Thermo Fisher Scientific, Waltham, MA, USA). Nuclei were stained with DAPI (Sigma-Aldrich). Fluorescent images were captured using a confocal laser scanning microscope (LSM510 META, Carl Zeiss, Oberkochen, Germany) with a 20× or 40× objective lens. In some experiments (Fig. 4d), 12 Z-stack images at 1.2-μm intervals were acquired using the confocal microscope with a 40× objective lens.

Luc assay. To measure the GLI-mediated transcriptional repression in response to cyclopamine, B16F10 cells were plated in 12-well plates at 8×10^4 cells per well, and were cotransfected with 950 ng of the Luc reporter vector (8xGLI-BS-Luc or 8xmGli-BS-Luc, kind gifts from Dr Hiroshi Sasaki, Kumamoto University, Kumamoto, Japan)[37] and 50 ng of the *Renilla* Luc control vector (pRL-TK-Luc, Promega) using Lipofectamine LTX with Plus reagent (Thermo Fisher Scientific). Six hours after transfection, the medium was changed, and the cells were treated with either vehicle (DMSO) or cyclopamine for 24 h. The cells were then lysed, and the Luc activity was measured as previously described.[34] To examine the effect of GLI1 overexpression on the potential promoters of *Snail1*, *Zeb1* and *Twist*1, 350 ng of the Luc reporter vector containing the potential promoter region, 140 ng of either pCL20c-CMV-EGFP or pCL20c-CMV-HA-GLI1, and 10 ng of pRL-TK-Luc were cotransfected into HEK293T cells plated in 12-well plates at 2×10^5 cells per well. Thirty-six hours after transfection, the cells were lysed, and subjected to Luc assays as described previously.[34]

Matrigel invasion assay. The cell invasion assay was carried out using Transwell chambers with inserts of an 8-μm pore size (Corning, Corning, NY, USA). The upper chamber was pre-coated with Matrigel (300 μg/mL, 100 μL per well for B16F10 cells; 200 μg/mL, 100 μL per well for MeWo cells, BD Biosciences, San Jose, CA, USA). NIH3T3-conditioned medium containing 10% FBS (for B16F10 cells) or EMEM complete growth medium supplemented with 10% FBS (for MeWo and G361 cells) was added to the lower chamber, which was pre-coated with 50 μL of fibronectin (50 μg/mL; Thermo Fisher Scientific), and then 1×10^5 cells were seeded on the upper chamber in serum-free medium containing 0.1% BSA. In some experiments (Fig. 1), cyclopamine was added to both the upper and lower chambers. At 24 h (for B16F10 cells) or 30 h (for MeWo and G361 cells) after seeding, the cells were fixed in 4% paraformaldehyde and stained with 0.1% crystal violet. Cells remaining on the upper side of the inserts were scraped with cotton swabs, and cells on the lower side were counted.

Cell migration assay. To measure the cell migration activity, wound-healing (for B16F10 cells) and Transwell chamber (for MeWo and G361 cells) assays were performed. B16F10 cells were replated at a saturation density (2×10^5 cells per well of a 12-well plate) in RPMI 1640 supplemented with 1% FBS, and incubated for 6 h. The plates were then scratched manually with a sterile pipette tip. After being washed with RPMI 1640, the wounded regions were allowed to heal for 12 h in RPMI 1640 medium supplemented with 1% FBS. The cell movements were monitored using a cultured cell monitoring system (CCM-1.4XYZ/CO2, Astec, Fukuoka, Japan). Video images were collected at 15-min intervals for 12 h. Transwell chamber migration assays were carried out as described above (Matrigel invasion assay) without pre-coating the upper chamber.
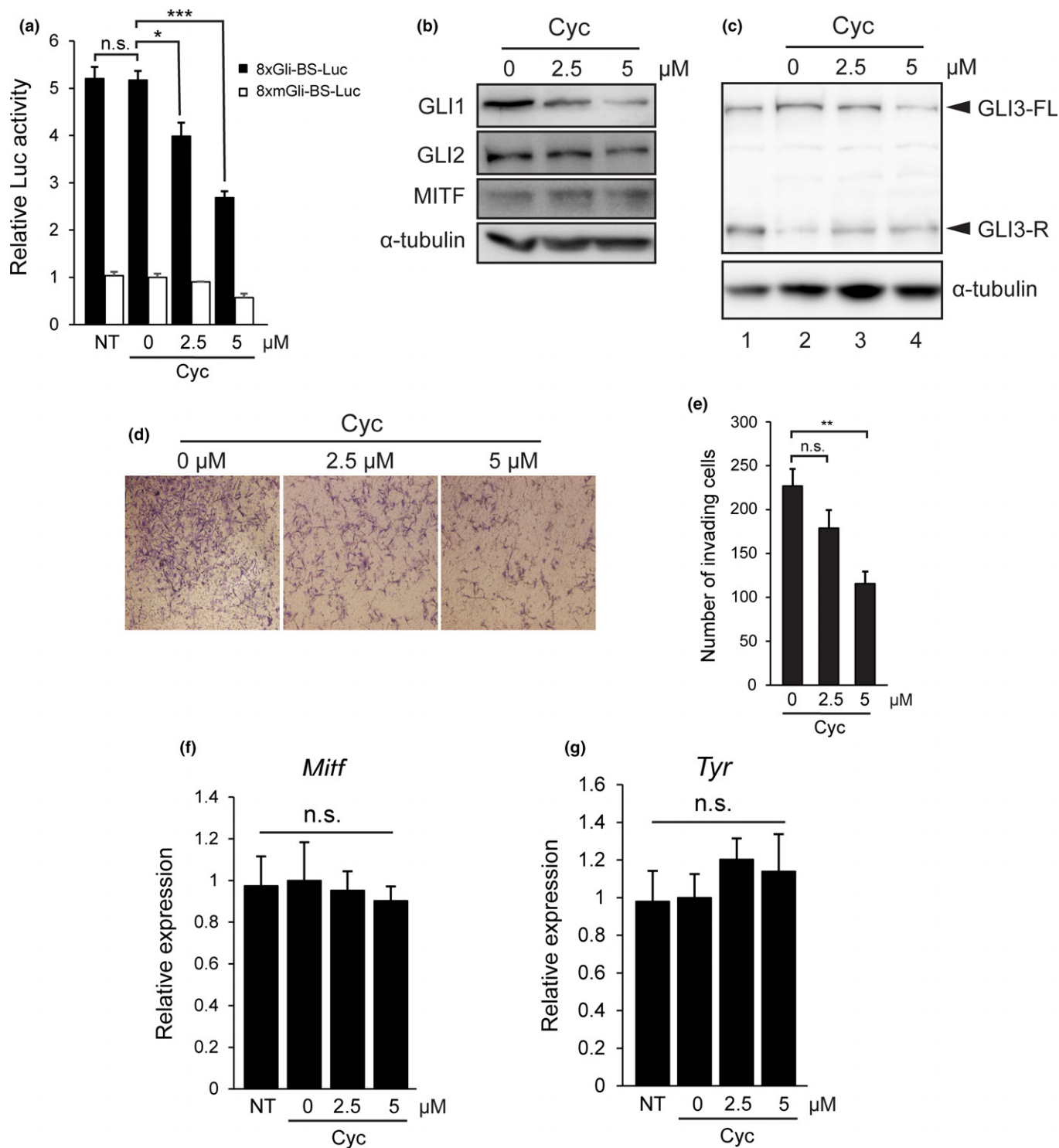
Fig. 1. Blockade of Shh signaling inhibits the invasion activity of melanoma cells. (a) B16F10 cells were cotransfected with a firefly Luc reporter plasmid containing GLI-binding sites (8xGli-BS-Luc) or mutated sites (8xmGli-BS-Luc) together with a *Renilla* Luc reporter plasmid, and were assayed for Luc activity, as described in the Materials and Methods. (b,c) B16F10 cells were treated with cyclopamine for 48 h, and were subjected to western blotting using anti-GLI1, anti-GLI2, anti-MITF (b) and anti-GLI3 (c) Abs. Lane 1, cell lysate prepared from mouse embryonic fibroblasts (MEF). α-tubulin, a loading control. (d) B16F10 cells were pre-treated with cyclopamine for 24 h, and were subjected to a Matrigel invasion assay. Representative images captured using a microscope (BX50, Olympus, Tokyo, Japan) are shown. (e) Quantification of the results in (d). The average numbers of invading cells from five randomly chosen fields acquired using a 20× objective lens are shown. (f,g) B16F10 cells were untreated or treated with cyclopamine for 48 h, and the relative mRNA levels of *Mitf* (f) and *Tyr* (g) were then measured by quantitative RT-PCR. The expression levels were normalized to *Gapdh*. Quantitative data are expressed as the mean ± SEM of three independent experiments. $*P < 0.05$; $**P < 0.01$; $***P < 0.001$; n.s., not significant; Cyc, cyclopamine; NT, untreated.
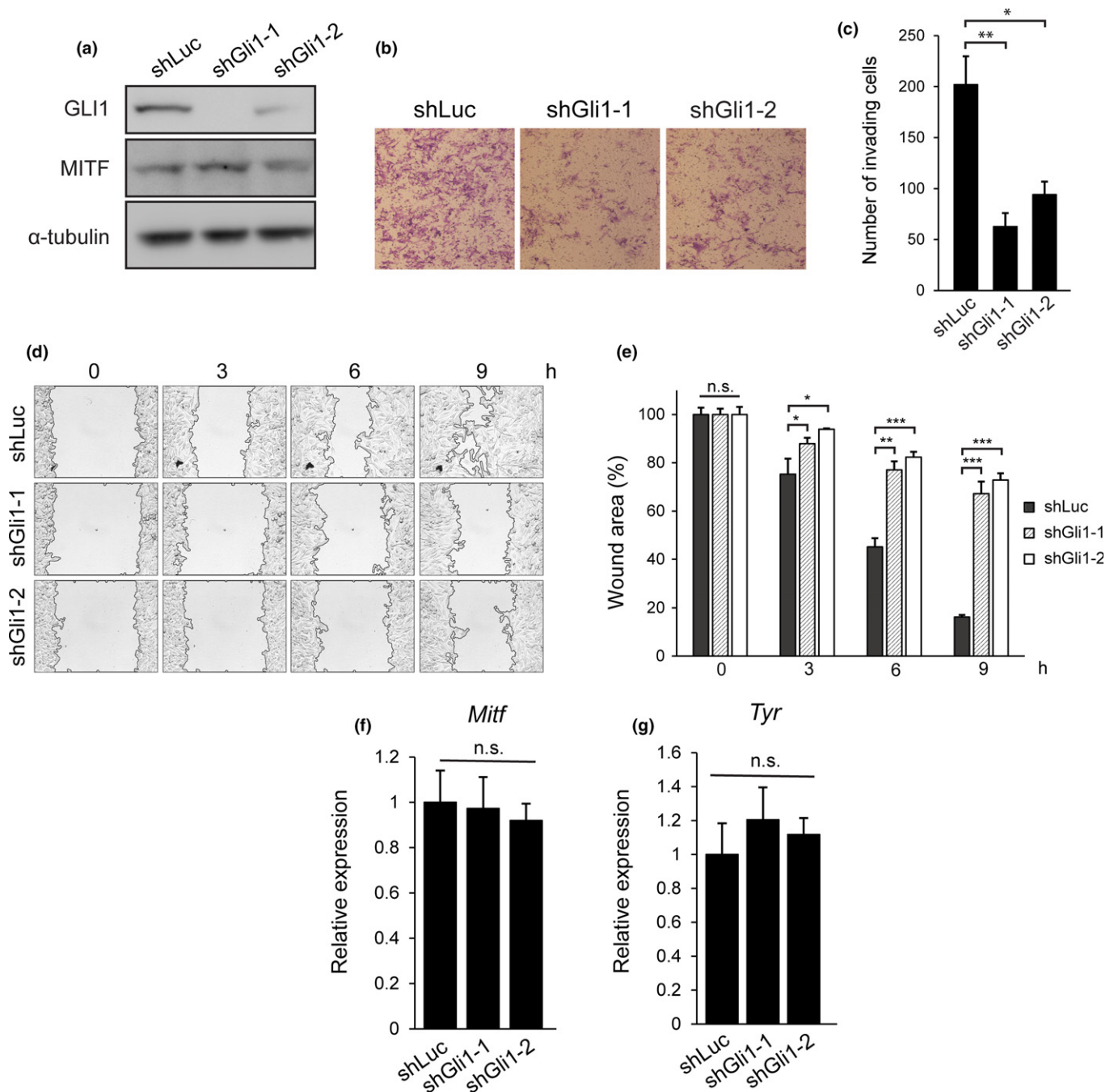
Fig. 2. *Gli1* knockdown (KD) inhibits the invasion and migration abilities of melanoma cells. (a) B16F10 cells were infected with lentiviral shLuc, shGli1-1 or shGli1-2 (termed B16F10_shLuc, B16F10_shGli1-1 and B16F10_shGli1-2 cells, respectively), and the protein levels of GLI1 and MITF were examined by western blotting using anti-GLI1 and anti-MITF Abs. α-tubulin, a loading control. (b) Matrigel invasion assays were performed as in Figure 1d, using B16F10_shLuc, B16F10_shGli1-1 and B16F10_shGli1-2 cells. Representative images of invading cells are shown. (c) Quantification of the results in (b), performed as described in Figure 1e. (d) B16F10_shLuc, B16F10_shGli1-1 and B16F10_shGli1-2 cells were analyzed by *in vitro* wound-healing assays. Phase-contrast time-lapse images at 0, 3, 6 and 9 h are shown. Curved black lines indicate the boundary between the unscratched and scratched areas. (e) Quantification of wound size using ImageJ software (NIH). (f,g) Relative mRNA levels of *Mitf* (f) and *Tyr* (g) in B16F10_shLuc, B16F10_shGli1-1 and B16F10_shGli1-2 cells were measured by quantitative RT-PCR as in Figure 1e,f. $*P < 0.05$; $**P < 0.01$; $***P < 0.001$; n.s., not significant.

MTT assay. The MTT assay was used to examine cell viability. B16F10, MeWo or G361 cells were seeded in 24-well plates (8×10^4 cells per well), and incubated overnight. The medium was then changed to serum-free medium containing 0.1% BSA, and the cells were incubated for 24 h to mimic the Matrigel invasion assay described above. In some experiments (Fig. S1), cyclopamine was added to the culture medium. The cells were washed with PBS and incubated with MTT solution (0.5 mg/mL, Sigma) for 1 h. The resulting insoluble formazan was dissolved in 0.04 N HCl in isopropanol, and the absorbance at 595 nm was measured.

ChIP assays. ChIP assays were performed essentially as described previously.[38] B16F10 cells were cross-linked with formaldehyde, lysed, and sonicated using a Bioruptor
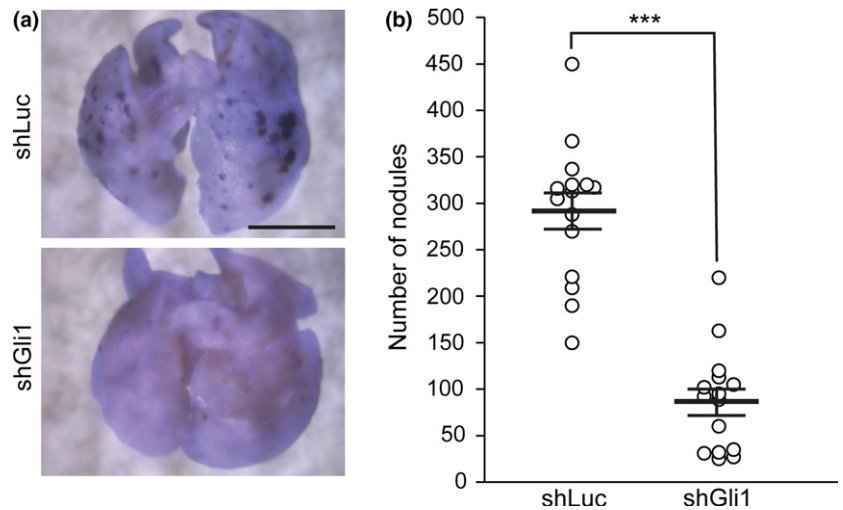
Fig. 3. *Gli1* knockdown (KD) decreases the lung metastasis ability of B16F10 cells. (a) Representative images of the lungs of mice injected with B16F10_shLuc or B16F10_shGli1-1 cells. (b) Each open circle denotes the number of nodules representing the pulmonary metastasis ability of B16F10_shLuc and B16F10_shGli1-1 cells in mice treated as in (a). Data are the means $\pm$ SEM ($n = 15$ mice per group). ***$P < 0.001$. Scale bar, 0.5 cm.

sonicator (CosmoBio, Tokyo, Japan). The lysates were immunoprecipitated with the rabbit anti-GLI1 H300 Ab (sc-20687; Santa Cruz Biotechnology) or control rabbit IgG (011-000-003; Jackson ImmunoResearch Laboratory, West Grove, PA, USA), and the precipitated DNA was subjected to quantitative PCR (qPCR). Primers used for the qPCR are listed in Table S3.

Animal experiments. All experimental procedures involving mice were approved by the Institutional Animal Care and Use Committee of Kanazawa University. To evaluate the cells' metastatic ability, *in vivo* metastasis assays were performed in mice. B16F10 cells suspended in 200 μL of PBS containing 5% FBS were injected into the tail vein of 8-week-old male C57BL/6 mice (Sankyo Labo Service, Tokyo, Japan). The mice were sacrificed 14 days after the inoculation, and the lungs were fixed in 10% formalin. The metastatic foci in the lungs were counted under a microscope to evaluate the development of pulmonary metastasis.

Statistical analysis. Significance was determined using a two-tailed unpaired Student's *t*-test. Values of $P < 0.05$ were considered to be statistically significant.

Results

Blockade of Shh signaling inhibits the invasion ability of melanoma cells without affecting their MITF expression and activity. We first examined the role of Shh signaling in maintaining the invasive phenotype of melanoma cells. We used the highly metastatic murine melanoma cell line B16F10, which is widely used as a model system to study melanoma biology, and blocked the Shh-GLI signaling pathway using cyclopamine, an inhibitor of SMO. B16F10 cells treated with cyclopamine at relatively low concentrations, 2.5 and 5 μM, showed decreased levels of GLI1 protein and of GLI-mediated transcriptional

activity, in a dose-dependent manner (Fig. 1a,b). We also examined the expression of GLI2 and GLI3, which mainly function as a transcriptional activator and repressor, respectively. GLI2 was decreased by cyclopamine, but to a lesser degree than GLI1 (Fig. 1b). The processed, repressive form of GLI3 (GLI3-R) was slightly increased, and full-length GLI3 (GLI3-FL) was decreased, in cyclopamine-treated B16F10 cells in a dose-dependent manner (Fig. 1c). We then performed an *in vitro* invasion assay. As shown in Figure 1d and e, blocking Shh signaling with cyclopamine caused a dose-dependent decrease in invasion activity, in which a statistically significant difference was observed between cyclopamine-untreated and cyclopamine-treated B16F10 cells at 5 μM, but not 2.5 μM. There was no significant effect of cyclopamine at either concentration on cell viability under the conditions used for the invasion assay (Fig. S1).

The invasive phenotype of melanoma cells is often characterized by low levels of MITF. Therefore, we examined the protein levels of MITF by western blotting in cyclopamine-treated B16F10 cells at 2.5 and 5 μM, and compared it to that in cyclopamine-untreated cells. Unexpectedly, the MITF levels were comparable among these cells (Fig. 1b). There were also no significant differences in the mRNA levels of *Mitf* and *Tyrosinase* (*Tyr*), a MITF-target gene, in these cells (Fig. 1f, g). To rule out the possibility that the transcriptional regulation of the *Mitf* gene was impaired in the B16F10 cells, we stimulated the cells with forskolin, a cAMP-elevating reagent known to induce *Mitf* promoter activity. As expected, the protein and mRNA levels of MITF and *Tyr* were increased, respectively, in the forskolin-treated B16F10 cells (Fig. S2). Taken together, these results indicated that blocking the Shh signaling by cyclopamine inhibits the invasion ability of B16F10 melanoma cells without affecting their MITF expression and activity.

Fig. 4. *Gli1* knockdown (KD) induces reversal of the mesenchymal-like phenotype. (a) B16F10_shLuc and B16F10_shGli1-1 cells, which express enhanced green fluorescent protein (EGFP), were double stained with rhodamine-phalloidin and DAPI. Lower panels show higher-magnification images of the boxed areas in the upper panels. (b) Relative mRNA levels of *E-cadherin* (*Cdh1*) in the B16F10_shLuc and B16F10_shGli1-1 cells were measured by quantitative RT-PCR (qRT-PCR) as in Figure 1e,f. (c) The protein levels of E-cadherin in B16F10_shLuc and B16F10_shGli1-1 cells were examined by western blotting using an anti-E-cadherin Ab. α-tubulin, a loading control. (d) B16F10_shLuc and B16F10_shGli1-1 cells were double stained with DAPI and an anti-E-cadherin Ab. Lower panels show higher-magnification Z-stack images of the boxed areas in the upper panels. Z-stack images were acquired using a confocal microscope as described in the Materials and Methods. (e) Relative mRNA levels of *N-cadherin* (*Cdh2*), *vimentin* (*Vim*) and *fibronectin* (*Fn1*) in B16F10_shLuc and B16F10_shGli1 cells were measured by qRT-PCR as in (b). *$P < 0.05$; **$P < 0.01$. Scale bars, 100 μm.
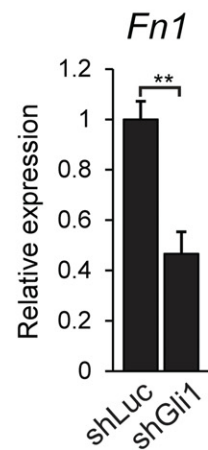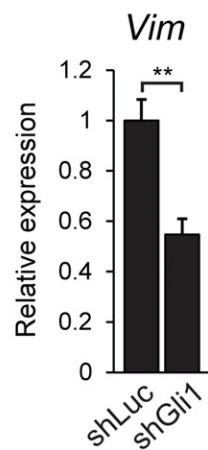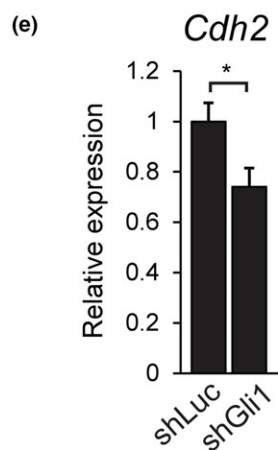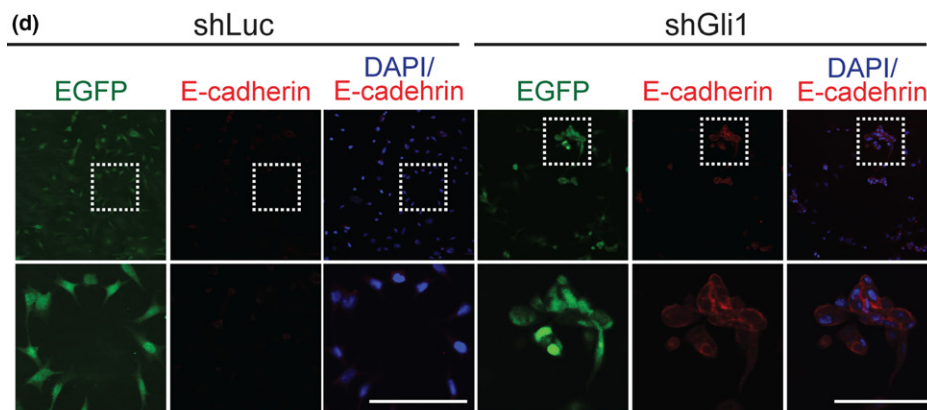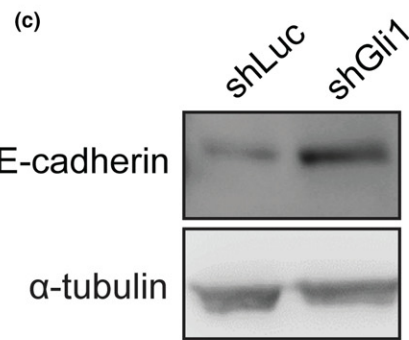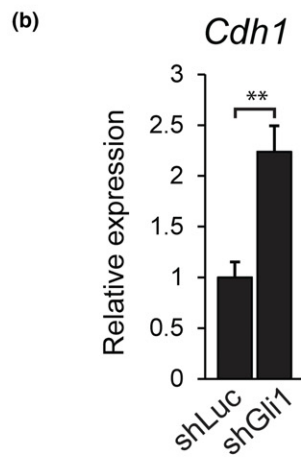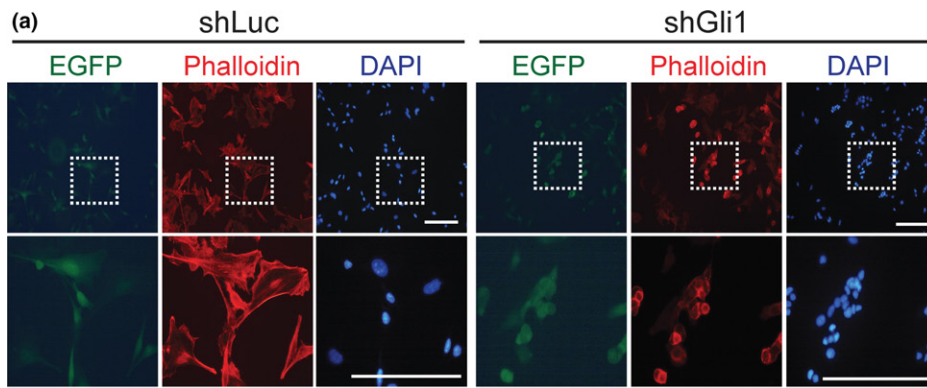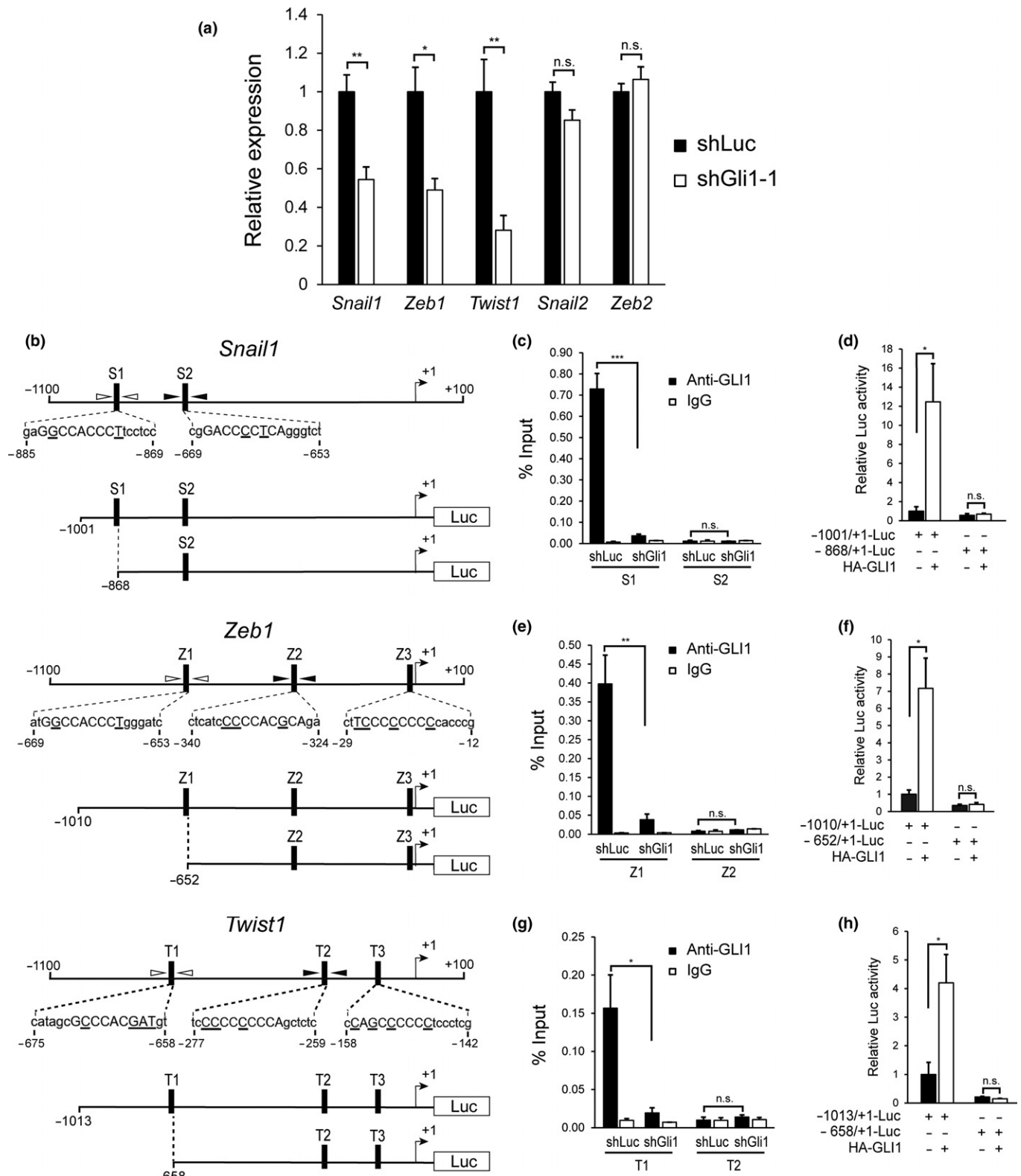
Fig. 5. GLI1 transcriptionally regulates the expression of *Snail1*, *Zeb1* and *Twist1*. (a) Expression of epithelial-to-mesenchymal transition-inducing transcription factors (EMT-TF) in *Gli1* KD B16F10 cells. Relative mRNA levels of *Snail1*, *Snail2*, *Zeb1*, *Zeb2* and *Twist1* in B16F10_shLuc and B16F10_shGli1-1 cells were measured by qRT-PCR as in Figure 1e,f. (b) Scheme of the potential promoter regions of *Snail1*, *Zeb1* and *Twist1*, and the Luc reporter. Numbers indicate the position relative to the transcriptional start sites (+1). Closed vertical boxes represent putative GLI-binding sites. Core sequences of the GLI-binding motif are shown by uppercase letters, in which the underlined nucleotides differ from the consensus sequences. Open and closed arrowheads indicate qPCR primers. (c–h) ChIP and quantitative PCR (c,e,g), and Luc (d,f,h) assays were performed as described in the Materials and Methods. *$P < 0.05$; **$P < 0.01$; ***$P < 0.001$; n.s., not significant.

***Gli1* knockdown inhibits the invasion ability and migration of melanoma cells, independently of the regulation of MITF expression and activity.** We next asked whether GLI1, a reliable marker for Shh pathway activity,[39,40] is responsible for the invasive phenotype of melanoma cells. We established *Gli1* KD B16F10 cells using two *Gli1*-targeting lentiviral shRNA (shGli1-1 and shGli1-2) to exclude off-target effects (Fig. 2a), and then examined the invasion ability and migration of the *Gli1* KD cells. The invasion ability of the KD cells was substantially reduced compared to that of control B16F10 cells expressing a *Luc*-targeting lentiviral shRNA (shLuc; Fig. 2b,c). No significant differences in viability were detected between the shLuc-expressing and shGli1-expressing B16F10 cells under the culture conditions used for the invasion assay (Fig. S3a). In addition, overexpressing GLI1 in B16F10 cells significantly increased the cells' invasion activity (Fig. S4). The cell migration activity, which was evaluated by an *in vitro* wound-healing assay, was also inhibited by knocking down *Gli1* (Fig. 2d,e). We then analyzed the expression levels of MITF (protein and mRNA) and its target gene *Tyr* in the *Gli1* KD B16F10 cells, and found that the MITF and *Tyr* levels were unchanged (Fig. 2a,f,g), as seen in the cyclopamine-treated B16F10 cells (Fig. 1b,f,g). Similar effects on the cell migration and invasion abilities and the MITF expression and activity were obtained using *GLI1* KD MeWo (wild-type BRAF/NRAS) and G361 (BRAF^{V600E}) cells, which are metastatic human melanoma cell lines (Fig. S5). Taken together, these results strongly suggested that GLI1 plays a crucial role in maintaining the invasive phenotype of melanoma cells, independently of the regulation of MITF expression and activity.

***Gli1* knockdown prevents the lung metastasis ability of B16F10 cells.** The results of the *in vitro* invasion and migration assays obtained with *Gli1* KD melanoma cells (Figs 2 and S5) prompted us to examine the metastatic ability of the KD cells *in vivo*. We performed an experimental *in vivo* metastasis assay, in which B16F10 cells expressing shLuc (control) or shGli1 were injected into the mouse tail vein, and lung metastasis was evaluated. There were many fewer metastatic nodules in the lungs of mice injected with shGli1-expressing cells than in the lungs of control B16F10-injected mice (Fig. 3), indicating that *Gli1* KD decreases the lung metastasis ability of B16F10 cells.

***Gli1* knockdown induces a reversal of the mesenchymal-like phenotype.** During analysis, we noticed that the *Gli1* KD B16F10 cells tended to associate with each other, and that they changed morphologically. Further examination by phalloidin staining showed that stress fiber formation was severely inhibited in the *Gli1* KD cells (Fig. 4a). Consistent with the changes in morphology and cytoskeletal structures, the expression levels of E-cadherin (protein and mRNA) were substantially increased, with the E-cadherin protein being predominantly localized to areas of cell–cell contact, in the *Gli1* KD cells (Fig. 4b–d). Furthermore, the mRNA expression levels of mesenchymal markers, such as N-cadherin and vimentin, were significantly decreased in the *Gli1* KD cells compared to the shLuc-expressing control cells (Fig. 4e). Similar expression profiles of E-cadherin and mesenchymal markers were obtained using MeWo and G361 cells (Fig. S6). These results may indicate that GLI1 regulates a subset of EMT-TF to prevent the reverse transition from a mesenchymal-like to an epithelial-like phenotype.

GLI1 transcriptionally regulates the expression of *Snail1*, *Zeb1* and *Twist1*. We further investigated whether GLI1 modulates the expression of key EMT-TF, including SNAIL and ZEB family members. As shown in Figure 5a, the mRNA levels of *Snail1*, *Zeb1* and *Twist1* were significantly decreased in the *Gli1* KD B16F10 cells compared to the control B16F10 cells, whereas no significant differences in the *Snail2* or *Zeb2* mRNA levels were observed between the *Gli1* KD and control cells. Using the MatInspector software,[41] we identified several putative GLI-binding sites within the 1-kb upstream region of the transcriptional start sites of *Snail1*, *Zeb1* and *Twist1* (termed S1 and S2 for *Snail1*; Z1, Z2 and Z3 for *Zeb1*; and T1, T2 and T3 for *Twist1*; see Fig. 5b). We then conducted ChIP assays with an anti-GLI1 Ab in B16F10 cells. The precipitated DNA were analyzed by qPCR using primers specific for the GLI1-binding sites (see Table S3 and Fig. S7). However, because the regions around Z3 and T3, which are close to transcriptional start sites, are GC-rich, we were unable to design specific primer sets and, therefore, did not perform ChIP experiments for them. The ChIP results revealed that GLI1 bound significantly to S1, Z1 and T1, but not to S2, Z2 or T2 (Fig. 5c,e,g). We then examined the effect of GLI1 overexpression on the potential promoters of *Snail1*, *Zeb1* and *Twist1* using reporter assays, and found that GLI1 overexpression substantially enhanced the promoter activities of the 1-kb regions. The activities were not significantly increased when the regions' corresponding deletion derivatives were used (Fig. 5d, f,h). Collectively, these results strongly suggest that GLI1 binds directly to the promoters of *Snail1*, *Zeb1* and *Twist1*, and regulates their expression. In addition, we found a significant co-occurrence between *GLI1* and *ZEB1* ($P = 0.002$) and between *GLI1* and *SNAIL1* ($P = 0.004$) by analyzing the TCGA cutaneous melanoma dataset (287 samples with RNA sequencing expression data) through the cBioPortal for cancer genomic data.[42,43]

Discussion

Microphthalmia-associated transcription factor is a key molecule that regulates heterogeneity in melanoma, and the so-called MITF rheostat model has become widely accepted in melanoma biology. In the present study, we demonstrated for the first time that the transcription factor GLI1 plays an important role in maintaining the invasive phenotype of melanoma cells without affecting the MITF expression and activity. We also showed that GLI1 prevents the reversal of the mesenchymal-like phenotype of melanoma cells, most likely by modulating a subset of EMT-TF. These findings provide new insight into how a high degree of heterogeneity and plasticity is achieved and regulated in melanoma.

Microenvironmental factors, such as hypoxia or TGF-β, are known to influence both MITF expression and the phenotype switching of melanoma cells.[17,20,44–47] In addition, Pierrat *et al.*[44] report that *Mitf* is downregulated by GLI2 and TGF-β to antagonize the MITF activity. Furthermore, Faião-Flores *et al.*[47] show that the GLI1 and GLI2 expressions increase upon the acquisition of BRAF inhibitor (BRAFi) resistance in melanoma cell lines and patient melanoma samples, where again the inverse correlation between GLI1/2 and MITF expression is observed. In contrast, in this study we found that GLI1 exerts its function with little or no effect on the MITF expression and activity. Nevertheless, the results of the present study are not inconsistent with previous studies, considering the following points. First, *Gli1* is a direct transcriptional target of GLI2.[48,49] Second, GANT61, a pharmacological inhibitor used in the previous studies, inhibits both the GLI1 and

GLI2 activities.[50,51] Accordingly, as explained by Faião-Flores et al.[47] the increased expression of GLI2 by TGF-β through a non-canonical Shh pathway results in an increase and decrease in GLI1 and MITF expression, respectively, which can be canceled by GANT61. Finally, although GLI1 and GLI2 have very similar consensus DNA-binding sites,[52] GLI2, but not GLI1, may specifically regulate *Mitf* transcription along with GLI2-interacting cofactors, which have been proposed by Eichberger et al.[53] Taken together, it is conceivable that GLI1 and GLI2 play distinct roles in the transcriptional regulation of *Mitf*.

Recent studies have shown that a switch in the EMT-TF expression pattern from SNAIL2^{high}/ZEB2^{high}/TWIST1^{low}/ZEB1^{low} to SNAIL2^{low}/ZEB2^{low}/TWIST1^{high}/ZEB1^{high} occurs during melanoma progression.[24,25] Caramel et al.[24] further demonstrate that EMT-TF reprograming is associated with decreased MITF expression and activity. In addition, Richard et al.[54] report that ZEB1 plays a key role as a major driver of melanoma cell plasticity and phenotypic resistance to BRAFi, and that *Zeb1* KD increases the sensitivity to BRAFi in both MITF^{low} and MITF^{high} cellular contexts. In this study, in contrast, we found that *Gli1* KD induced a mesenchymal–epithelial-like transition in melanoma cells, which was accompanied by severely decreased invasive and migratory properties, and by an increased expression of E-cadherin and downregulation of mesenchymal markers. We also observed decreased mRNA levels of *Snail1*, *Zeb1* and *Twist1*, but not of *Snail2* or *Zeb2*, in the *Gli1* KD melanoma cells. It is reported that SNAIL1 and TWIST1 cooperatively control *Zeb1* expression during EMT in epithelial cells.[55] Taken together with the results of our ChIP and Luc reporter assays (Fig. 5), it is conceivable that GLI1 directly regulates the transcriptional expression of a subset of EMT-TF, including *Snail1* and *Twist1*, as in non-melanoma cancer cells,[56,57] to maintain the invasive activity of melanoma cells through MITF-independent mechanisms. Further studies are needed to clarify this issue.

An increased expression of *Gli1* has been observed in BRAFi-resistant melanoma cells and patient samples,[47] as well as during melanoma progression.[58] Taken together with our present results, GLI1 may play a role in generating a high level of intratumor heterogeneity in melanoma. Targeting GLI1 may, therefore, be an effective approach for melanoma therapy. Indeed, accumulating evidence suggests that GLI antagonists, of which GANT61 has been most extensively studied *in vitro* and in animal models, are promising therapeutic candidates for a wide range of cancers, including melanoma.[59] However, GANT61 and other GLI antagonists, such as arsenic trioxide,[59] inhibit the activity not only of GLI1, but also of GLI2, which is a negative regulator of MITF expression and function, as described above. MITF plays an important, but complex role in melanoma biology, in which MITF-low melanomas appear to be more invasive and MITF-high melanomas more proliferative.[24,25] Our present findings suggest that GLI1-specific inhibitors may be more beneficial for cancer patients than GLI1/2 antagonists. Further studies are needed to investigate and develop such therapeutics.

Acknowledgments

Disclosure Statement

The authors have no conflict of interest.

References

1 Miller AJ, Mihm MC Jr. Melanoma. *N Engl J Med* 2006; **355**: 51–65.
2 Tsao H, Chin L, Garraway LA, Fisher DE. Melanoma: from mutations to medicine. *Genes Dev* 2012; **26**: 1131–55.
3 Davies H, Bignell GR, Cox C et al. Mutations of the BRAF gene in human cancer. *Nature* 2002; **417**: 949–54.
4 Sosman JA, Kim KB, Schuchter L et al. Survival in BRAF V600-mutant advanced melanoma treated with vemurafenib. *N Engl J Med* 2012; **366**: 707–14.
5 Chapman PB, Hauschild A, Robert C et al. Improved survival with vemurafenib in melanoma with BRAF V600E mutation. *N Engl J Med* 2011; **364**: 2507–16.
6 Flaherty KT, Infante JR, Daud A et al. Combined BRAF and MEK inhibition in melanoma with BRAF V600 mutations. *N Engl J Med* 2012; **367**: 1694–703.
7 Lito P, Rosen N, Solit DB. Tumor adaptation and resistance to RAF inhibitors. *Nat Med* 2013; **19**: 1401–9.
8 Van Allen EM, Wagle N, Sucker A et al. The genetic landscape of clinical resistance to RAF inhibition in metastatic melanoma. *Cancer Discov* 2014; **4**: 94–109.
9 Holderfield M, Deuker MM, McCormick F, McMahon M. Targeting RAF kinases for cancer therapy: BRAF-mutated melanoma and beyond. *Nat Rev Cancer* 2014; **14**: 455–67.
10 Long GV, Stroyakovskiy D, Gogas H et al. Combined BRAF and MEK inhibition versus BRAF inhibition alone in melanoma. *N Engl J Med* 2014; **371**: 1877–88.
11 Hamid O, Robert C, Daud A et al. Safety and tumor responses with lambrolizumab (anti-PD-1) in melanoma. *N Engl J Med* 2013; **369**: 134–44.
12 Robert C, Ribas A, Wolchok JD et al. Anti-programmed-death-receptor-1 treatment with pembrolizumab in ipilimumab-refractory advanced melanoma: a randomised dose-comparison cohort of a phase 1 trial. *Lancet* 2014; **384**: 1109–17.
13 Ribas A, Hamid O, Daud A et al. Association of pembrolizumab with tumor response and survival among patients with advanced melanoma. *JAMA* 2016; **315**: 1600–9.
14 Zaretsky JM, Garcia-Diaz A, Shin DS et al. Mutations associated with acquired resistance to PD-1 blockade in melanoma. *N Engl J Med* 2016; **375**: 819–29.
15 Jazirehi AR, Lim A, Dinh T. PD-1 inhibition and treatment of advanced melanoma-role of pembrolizumab. *Am J Cancer Res* 2016; **6**: 2117–28.
16 Hoek KS, Eichhoff OM, Schlegel NC et al. *In vivo* switching of human melanoma cells between proliferative and invasive states. *Cancer Res* 2008; **68**: 650–6.
17 Hoek KS, Goding CR. Cancer stem cells versus phenotype-switching in melanoma. *Pigment Cell Melanoma Res* 2010; **23**: 746–59.
18 Li FZ, Dhillon AS, Anderson RL, McArthur G, Ferrao PT. Phenotype switching in melanoma: implications for progression and therapy. *Front Oncol* 2015; **5**: 31.
19 Goding CR. Commentary. A picture of *Mitf* in melanoma immortality. *Oncogene* 2011; **30**: 2304–6.
20 Vandamme N, Berx G. Melanoma cells revive an embryonic transcriptional network to dictate phenotypic heterogeneity. *Front Oncol* 2014; **4**: 352.
21 De Craene B, Berx G. Regulatory networks defining EMT during cancer initiation and progression. *Nat Rev Cancer* 2013; **13**: 97–110.
22 Lamouille S, Xu J, Derynck R. Molecular mechanisms of epithelial–mesenchymal transition. *Nat Rev Mol Cell Biol* 2014; **15**: 178–96.
23 Ye X, Weinberg RA. Epithelial–mesenchymal plasticity: a central regulator of cancer progression. *Trends Cell Biol* 2015; **25**: 675–86.

24 Caramel J, Papadogeorgakis E, Hill L *et al.* A switch in the expression of embryonic EMT-inducers drives the development of malignant melanoma. *Cancer Cell* 2013; **24**: 466–80.

25 Denecker G, Vandamme N, Akay O *et al.* Identification of a ZEB2-MITF-ZEB1 transcriptional network that controls melanogenesis and melanoma progression. *Cell Death Differ* 2014; **21**: 1250–61.

26 Stecca B, Mas C, Clement V *et al.* Melanomas require HEDGEHOG-GLI signaling regulated by interactions between GLI1 and the RAS-MEK/AKT pathways. *Proc Natl Acad Sci USA* 2007; **104**: 5895–900.

27 Teglund S, Toftgård R. Hedgehog beyond medulloblastoma and basal cell carcinoma. *Biochim Biophys Acta* 2010; **1805**: 181–208.

28 Briscoe J, Thérond PP. The mechanisms of Hedgehog signalling and its roles in development and disease. *Nat Rev Mol Cell Biol* 2013; **14**: 416–29.

29 Pandolfi S, Stecca B. Cooperative integration between HEDGEHOG-GLI signalling and other oncogenic pathways: implications for cancer therapy. *Expert Rev Mol Med* 2015; **17**: e5.

30 Dennler S, André J, Alexaki I *et al.* Induction of sonic hedgehog mediators by transforming growth factor-beta: Smad3-dependent activation of Gli2 and Gli1 expression *in vitro* and *in vivo. Cancer Res* 2007; **67**: 6981–6.

31 Lei J, Fan L, Wei G *et al.* Gli-1 is crucial for hypoxia-induced epithelial–mesenchymal transition and invasion of breast cancer. *Tumour Biol* 2015; **36**: 3119–26.

32 Wang X, Zhao F, He X *et al.* Combining TGF-β1 knockdown and miR200c administration to optimize antitumor efficacy of B16F10/GPI-IL-21 vaccine. *Oncotarget* 2015; **6**: 12493–504.

33 Tuvshintugs B, Sato T, Enkhtuya R, Yamashita K, Yoshioka K. JSAP1 and JLP are required for ARF6 localization to the midbody in cytokinesis. *Genes Cells* 2014; **19**: 692–703.

34 Sato T, Torashima T, Sugihara K, Hirai H, Asano M, Yoshioka K. The scaffold protein JSAP1 regulates proliferation and differentiation of cerebellar granule cell precursors by modulating JNK signaling. *Mol Cell Neurosci* 2008; **39**: 569–78.

35 Sato T, Ishikawa M, Mochizuki M *et al.* JSAP1/JIP3 and JLP regulate kinesin-1-dependent axonal transport to prevent neuronal degeneration. *Cell Death Differ* 2015; **22**: 1260–74.

36 Takino T, Nakada M, Miyamori H *et al.* JSAP1/JIP3 cooperates with focal adhesion kinase to regulate c-Jun N-terminal kinase and cell migration. *J Biol Chem* 2005; **280**: 37772–81.

37 Sasaki H, Hui C, Nakafuku M, Kondoh H. A binding site for Gli proteins is essential for HNF-3beta floor plate enhancer activity in transgenics and can respond to Shh *in vitro. Development* 1997; **124**: 1313–22.

38 Yoshida M, Ishimura A, Terashima M *et al.* PLU1 histone demethylase decreases the expression of KAT5 and enhances the invasive activity of the cells. *Biochem J* 2011; **437**: 555–64.

39 Lee J, Platt KA, Censullo P, Ruiz i Altaba A. Gli1 is a target of Sonic hedgehog that induces ventral neural tube development. *Development* 1997; **124**: 2537–52.

40 Hynes M, Stone DM, Dowd M *et al.* Control of cell pattern in the neural tube by the zinc finger transcription factor and oncogene Gli-1. *Neuron* 1997; **19**: 15–26.

41 Cartharius K, Frech K, Grote K *et al.* MatInspector and beyond: promoter analysis based on transcription factor binding sites. *Bioinformatics* 2005; **21**: 2933–42.

42 Cerami E, Gao J, Dogrusoz U *et al.* The cBio cancer genomics portal: an open platform for exploring multidimensional cancer genomics data. *Cancer Discov* 2012; **2**: 401–4.

43 Gao J, Aksoy BA, Dogrusoz U *et al.* Integrative analysis of complex cancer genomics and clinical profiles using the cBioPortal. *Sci Signal* 2013; **6**: pl1.

44 Pierrat MJ, Marsaud V, Mauviel A, Javelaud D. Expression of microphthalmia–associated transcription factor (MITF), which is critical for melanoma progression, is inhibited by both transcription factor GLI2 and transforming growth factor-β. *J Biol Chem* 2012; **287**: 17996–8004.

45 Cheli Y, Giuliano S, Fenouille N *et al.* Hypoxia and MITF control metastatic behaviour in mouse and human melanoma cells. *Oncogene* 2012; **31**: 2461–70.

46 Laugier F, Delyon J, André J, Bensussan A, Dumaz N. Hypoxia and MITF regulate KIT oncogenic properties in melanocytes. *Oncogene* 2016; **35**: 5070–7.

47 Faião-Flores F, Alves-Fernandes DK, Pennacchi PC *et al.* Targeting the hedgehog transcription factors GLI1 and GLI2 restores sensitivity to vemurafenib-resistant human melanoma cells. *Oncogene* 2017; **36**: 1849–61.

48 Regl G, Neill GW, Eichberger T *et al.* Human GLI2 and GLI1 are part of a positive feedback mechanism in Basal Cell Carcinoma. *Oncogene* 2002; **21**: 5529–39.

49 Ikram MS, Neill GW, Regl G *et al.* GLI2 is expressed in normal human epidermis and BCC and induces GLI1 expression by binding to its promoter. *J Invest Dermatol* 2004; **122**: 1503–9.

50 Lauth M, Bergström A, Shimokawa T, Toftgård R. Inhibition of GLI-mediated transcription and tumor cell growth by small-molecule antagonists. *Proc Natl Acad Sci USA* 2007; **104**: 8455–60.

51 Agyeman A, Jha BK, Mazumdar T, Houghton JA. Mode and specificity of binding of the small molecule GANT61 to GLI determines inhibition of GLI-DNA binding. *Oncotarget* 2014; **5**: 4492–503.

52 Hallikas O, Palin K, Sinjushina N *et al.* Genome-wide prediction of mammalian enhancers based on analysis of transcription-factor binding affinity. *Cell* 2006; **124**: 47–59.

53 Eichberger T, Kaser A, Pixner C *et al.* GLI2-specific transcriptional activation of the bone morphogenetic protein/activin antagonist follistatin in human epidermal cells. *J Biol Chem* 2008; **283**: 12426–37.

54 Richard G, Dalle S, Monet MA *et al.* ZEB1-mediated melanoma cell plasticity enhances resistance to MAPK inhibitors. *EMBO Mol Med* 2016; **8**: 1143–61.

55 Dave N, Guaita-Esteruelas S, Gutarra S *et al.* Functional cooperation between Snail1 and twist in the regulation of ZEB1 expression during epithelial to mesenchymal transition. *J Biol Chem* 2011; **286**: 12024–32.

56 Li X, Deng W, Nail CD *et al.* Snail induction is an early response to Gli1 that determines the efficiency of epithelial transformation. *Oncogene* 2006; **25**: 609–21.

57 Kong Y, Peng Y, Liu Y, Xin H, Zhan X, Tan W. Twist1 and Snail link Hedgehog signaling to tumor-initiating cell-like properties and acquired chemoresistance independently of ABC transporters. *Stem Cells* 2015; **33**: 1063–74.

58 Das S, Harris LG, Metge BJ *et al.* The hedgehog pathway transcription factor GLI1 promotes malignant behavior of cancer cells by up-regulating osteopontin. *J Biol Chem* 2009; **284**: 22888–97.

59 Gonnissen A, Isebaert S, Haustermans K. Targeting the Hedgehog signaling pathway in cancer: Beyond Smoothened. *Oncotarget* 2015; **6**: 13899–913.

Supporting Information

Additional Supporting Information may be found online in the supporting information tab for this article:

Fig. S1. Blockade of Shh signaling shows no significant effect on cell viability.

Fig. S2. Forskolin induces the expression of microphthalmia-associated transcription factor (MITF) protein and its target gene *Tyr*.

Fig. S3. *Gli1* knockdown (KD) shows no significant effects on melanoma cell viability.

Fig. S4. GLI1 overexpression enhances the invasion activity of B16F10 cells.

Fig. S5. *Gli1* knockdown (KD) induces a reversal of the mesenchymal-like phenotype in MeWo and G361 cells.

Fig. S6. Expression of E-cadherin and mesenchymal markers in *Gli1* knockdown (KD) MeWo and G361 cells.

Fig. S7. Primers used in ChIP assays, and agarose gels of PCR products.

Table S1. List of oligonucleotides for the shRNA constructs used in this study.

Table S2. List of quantitative RT-PCR primers used in this study.

Table S3. List of quantitative PCR primers used in this study.